Detection of Vapor Released from Sublimating Materials Encased in Porous Medium

Wenshuo Zhang [a], Eyal Zussman [b, *], Alexander L. Yarin [a, *]

[a] Department of Mechanical and Industrial Engineering, University of Illinois at Chicago, Chicago, Illinois 60607-7022, USA

[b] Faculty of Mechanical Engineering, Technion-Israel Institute of Technology, Haifa 32000, Israel

Abstract

Detection of materials encased in porous media is important in many applications and can be attempted via sensing vapor sublimating from them. Development of such sensors requires evaluation of vapor concentration expected at the free surface from materials encased at different depths. In the present work experiments are conducted with a model material, naphthalene, which is relatively easy to detect. One of the main aims of these experiments is, however, in the development of a comprehensive theory (also in the present work) which is applicable to any sublimating material. Accordingly, the data acquired using the model experimental material (naphthalene buried in sand or clay) is used here for verification of the theory.

An additional aim is related to the question whether it is possible to amplify the vapor flux reaching the free surface by means of suppression of its partial adsorption in the bulk. Using sand as a porous medium of interest, it is shown that it is possible to achieve this goal by dip coating of sand in polymer solution with a subsequent drying. In a modified sand with a dramatically reduced surface area of the grains smoothened by the polymer coating, vapor adsorption is dramatically suppressed, while vapor flux toward the free surface is dramatically increased, thus increasing the chances of detection.

1. Introduction

Vapor and gas transfer in porous medium is an important subject which is relevant in such applications as petroleum and natural gas exploration, mining, water vapor transport through soil layers, leakage and smoke detection, forensics, etc. In the latter case, which is of particular interest in the present work, an encased sublimating material might be buried or hidden in porous medium. Then, vapor/gas sublimating from such a source diffuses into the surrounding medium and is inevitably partially adsorbed in it. The adsorption processes in porous media, either chemisorption or physisorption, were studied with various materials, such as porous silica [1, 2], porous carbon [3, 4], as well as with fibrous materials [5, 6]. As a result several types of the adsorption isotherms were established to describe the adsorption/ desorption equilibria in different situations [7-11].

Vapor or gas diffusing through the encasing porous media and being partially adsorbed in the pores, can also partially achieve the free surface and be, in principle, detected there. It should be emphasized that a detectable vapor or gas release to the free surface could be delayed due to

the adsorption in the pores at the beginning of the process. Thus, it might be of interest to speed up this process and amplify the vapor release to the surface, which is one of the aims of the present work. Such detection methods as polymer-coated acoustic wave sensors [12], chromatography [13], hyperspectral imaging [14], etc. were demonstrated to be effective for unknown vapor detection and determination. Besides that, detection and concentration of known vapor accompanied by mass quantification are also important. The methods for detection of specific known vapor are quite mature now. Many kinds of vapor sensors and methods have been developed, such as polymer sensors [15], resonating microcantilevers [16], and methods employig carbon nanotubes [17,18]. However, these sensors still have limitations when the spatial spatial distribution of released vapor is in question. Sensors can relatively easily detect and measure vapor concentration if vapor is pumped through the sensor [19]. Still, to determine the vapor distribution by this method would be imprecise because it is impractical to collect and pump the vapor just from a specific location. Using the existing sensors it is also difficult to determine the source size, and/or the depth and the horizontal location of a buried source.

Some types of vapor sublimating from the original materials are relatively concentrated and easily adsorbed, which makes them ideal model materials. For example, naphthalene vapor, as a typical polycyclic aromatic hydrocarbon with a unique smell, was used as a model material in several experimental works [20-23]. Solid naphthalene yields a relatively high vapor concentration, since it sublimates at a relatively high rate. Its deposits in the form of white crystals can be detected to quantify the amount of vapor released from a porous medium. The albedo measurement or estimation was demonstrated to be an effective method to explore the surface texture, surface temperature variations, surface energy, etc. Such measurements either demand precise instruments, such as pyranometers [24] and scanning radiometers [25], or just a

photograph [26]. Using the photography-based method is a convenient way to estimate the albedo value. However, it demands an albedo value of a known object as a reference point, i.e. it is impossible to establish the actual brightness values. Accordingly, it leads to imprecisions and errors when this method is used for vapor quantification. Since the albedo value is positive and proportional to the corresponding pixel intensity value [27], the intensity value can be obtained directly from a photograph. Thus, measuring the photograph pixel intensity values for vapor quantification purposes would be a more precise method.

In the present work, the experiments with a naphthalene ball located in the original sand, where it sublimates and its vapor is adsorbed and diffuses through the pores toward the free surface where the detection takes place, are described in Section 2. Similar experiments with a naphthalene ball located in kaolinite (clay) are described in Section 3. The theoretical description of the process is given in Section 4, and its comparison with the experimental data is discussed in Section 5. Experiments with naphthalene sublimation and diffusion in a modified sand (coated with polymer or after it underwent another surface treatment) are covered in Section 6. Conclusions are drawn in Section 7.

2. Experiments with original sand

2.1. Materials and experimental setup

The volatile material used in this work is naphthalene, which was purchased from Enoz. Its purity was 99.95%. The 1.9 cm naphthalene balls were used as received. Another volatile material used was camphor balls of 1.9 cm, which were formed from Frontier camphor powder.

Sand purchased from Quikrete was used as a model granular porous medium. It was pre-treated by rinsing in ethanol before being used in the experiments to eliminate impurities. Then, the wet sand was fully dried under 100 °C and sieved with 0.212 mm to 1.4 mm sieves. Such a sand, which had not underwent any surface modification, except the elimination of impurities, is termed as the original sand. Kaolinite was purchased from Halaeveryday.

A hotplate was used, and a copper plate of $12"\times12"\times0.093"$ in dimensions was located on its surface in order to maintain the uniform surface temperature. A polycarbonate tank ($14\,\text{cm}\times13\,\text{cm}\times22.5\,\text{cm}$) to be filled with sand was located on top of it and the tank bottom temperature was sustained at 78 ºC (close to the melting temperature of naphthalene which is 80.26 ºC) to speed up the experiments. A naphthalene ball was placed at the tank bottom, and after that, the tank was filled with sand. Four different heights of sand filling (or vice versa, four different depths of the naphthalene ball location) were used, namely, h=3.0 cm, 4.5 cm, 5.5 cm and 7.0 cm. After 1 h, the temperature in the tank reached a steady value and then a 3M transparent film ($13\,\text{cm}\times12\,\text{cm}\times0.05\,\text{cm}$) was placed at the free surface of the sand layer to collect naphthalene vapor, which reached the surface. It was found that the naphthalene vapor was deposited on the film in the form of white crystals.

At the beginning of any experiment, there was a relatively long delay time during which no naphthalene deposition on the film was observed at all. Such a delay cannot be attributed to diffusion. Indeed, the diffusion delay would be of the order of h^2/D, where D is the diffusion coefficient of the naphthalene vapor in air. Taking for the estimate h=7.0 cm and D=0.1 cm^2/s, the diffusion delay would be of about 8 min, whereas the observed delay was about t_{delay}=161 h. Therefore, the observed delay was due to vapor adsorption on sand grains in the bulk. Only after

the adsorption process had saturated, vapor could reach the surface, and deposit on the film on the surface in the form of white crystals. Once the crystals started to appear on the film, 10 h of continuous experiment was conducted, in which the crystalline deposit was photographed every 2 h. Due to the insolubility of naphthalene in water, the transparent film was gently washed by D.I. water to remove the attached sand particles before each image was taken. Image J software was used to analyze the crystal images collected over time.

2.2. Experiments results

A 1.9 cm naphthalene ball was located in the middle of the tank bottom. In separate experiments the original sand filled the tank up to the heights h=3.0 cm, 4.5 cm, 5.5 cm and 7.0 cm. The corresponding images of the films on the free surfaces of these sand layers recorded at several subsequent time moments for the height h=3.0 cm are shown in Fig. 1. It shows that in the case of h=3.0 cm crystals of naphthalene on the film become visible in the middle, i.e. above the source (the naphthalene ball buried in the sand) after a delay t_{delay}=12 h. During the delay time, no deposit was collected at the surface, which means that the entire vapor flux was adsorbed in the sand bulk on the grain surfaces. Only when the adsorption process was fully saturated, vapor could diffuse to the free surface and form the deposit there. The time listed in the caption of Fig. 1 is reckoned from this delay time. It should be emphasized that the crystal clusters seemingly continued to grow, i.e. the deposit density increased in time.

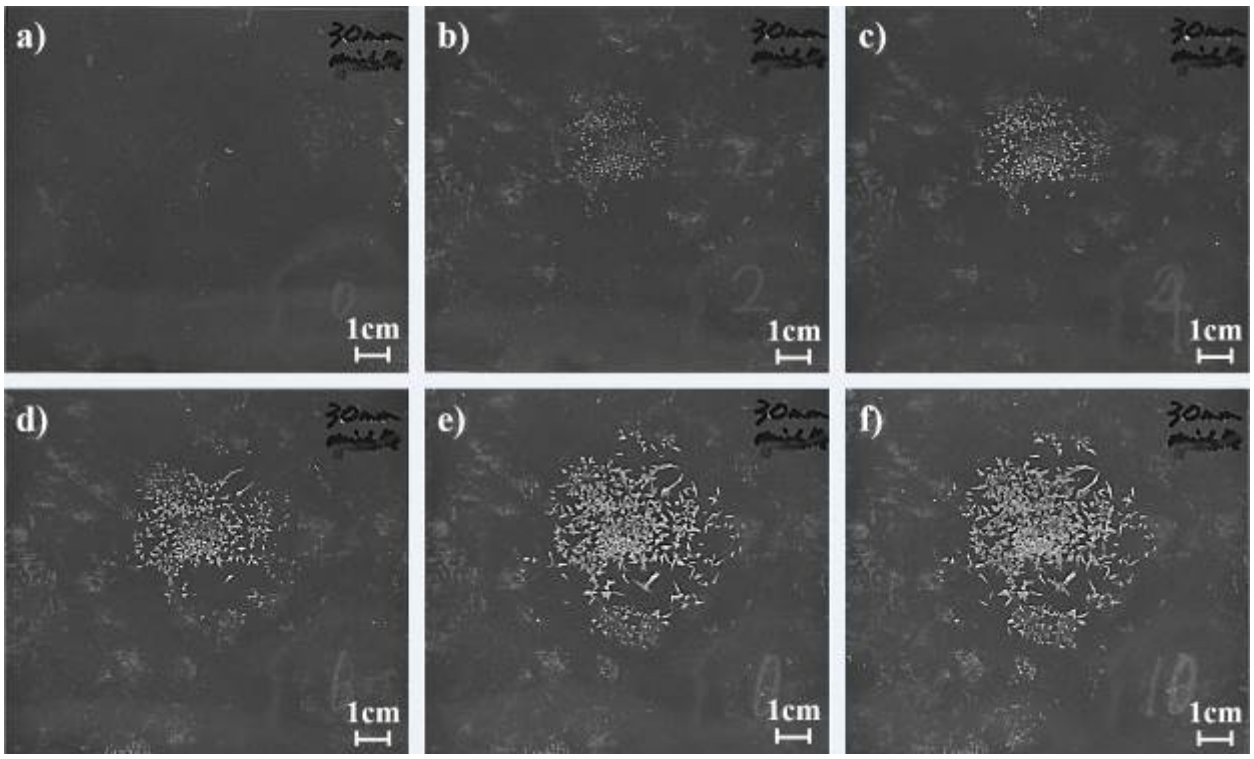

Figure 1. Morphology of naphthalene crystal deposits on transparent film at the free surface in the case of a 1.9 cm naphthalene ball buried in the middle under h=3 cm of the original sand: (a) at t=0, (b) at t=2 h, (c) at t=4 h, (d) at t=6 h, (e) at t=8 h, (f) at t=10 h. The time is reckoned from the delay time t_{delay}=12 h.

The area occupied by the naphthalene crystal deposits was outlined as shown, for example, in Fig. 2 and measured by counting the number of pixels inside. The cumulative results for all four heights of sand layer for the entire time of deposit observation (10 h in all the above-mentioned experiments) are shown in Fig. 3. It is seen that at least in the case of h=3 cm the area growth had saturated in 8 h (after the corresponding delay time t_{delay}=12 h). At higher values of h, the area saturation seemingly has not been reached, maybe because the area was not measured accurately enough to distinguish the peripheral fringes.

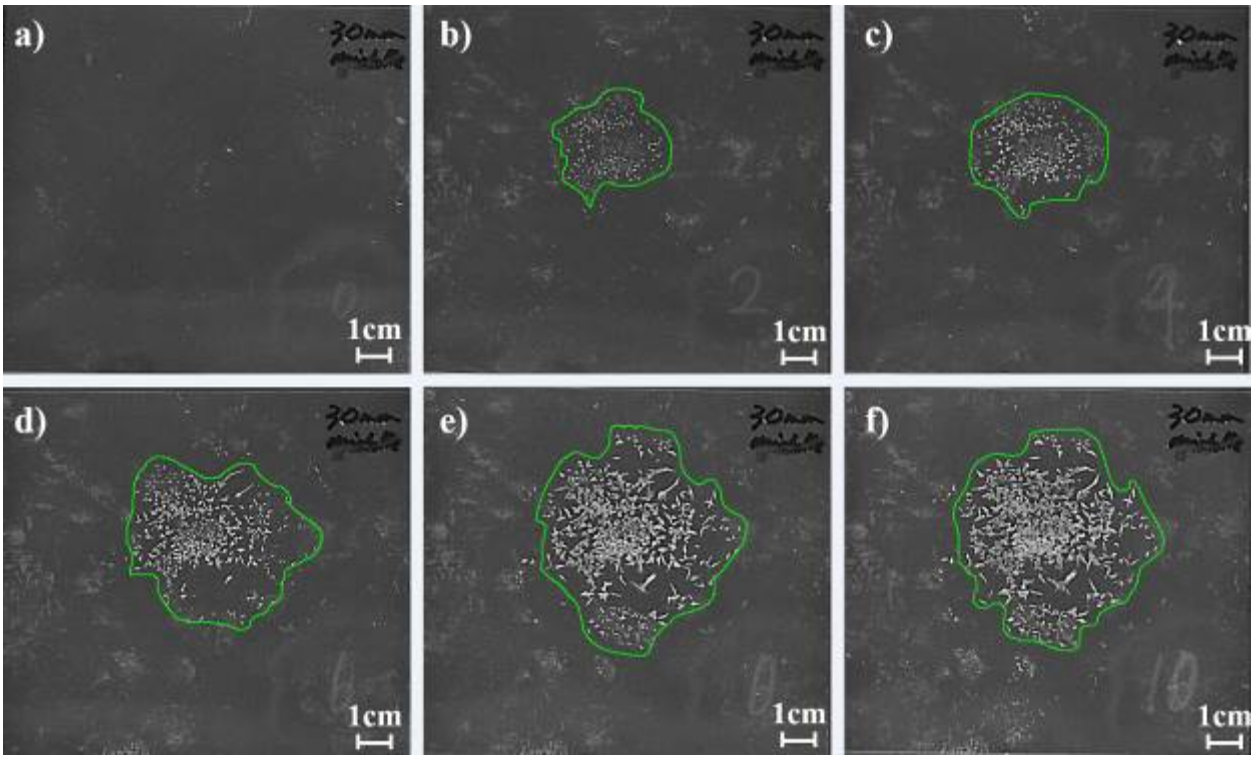

Figure 2. Measurement of the deposit surface area using the green outlines. The case of a 1.9 cm naphthalene ball buried in the middle under h=3 cm of the original sand: (a) at t=0, (b) at t=2 h, (c) at t=4 h, (d) at t=6 h, (e) at t=8 h, (f) at t=10 h. The time is reckoned from the delay time t_{delay}=12 h.

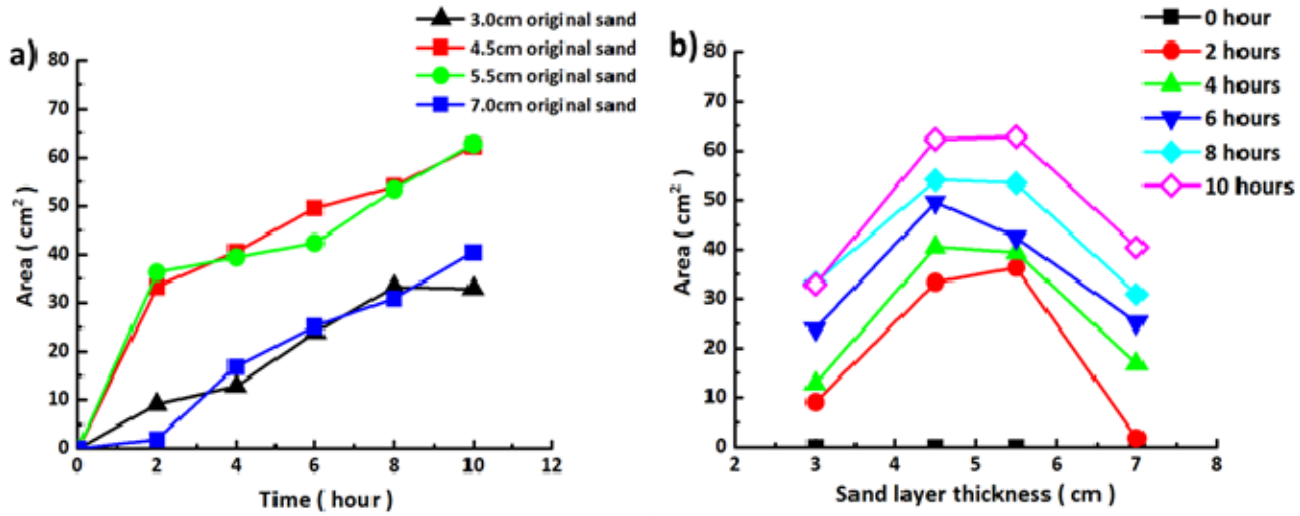

Figure 3. The measured deposit area for naphthalene crystal deposition. The case of the original sand, and a 1.9 cm naphthalene ball buried in the middle. (a) The area versus time, with time being reckoned from the delay times. (b) The area versus sand layer thickness. The experimental data is shown by symbols and spanned by lines.

2.3. Quantification of the amount of collected crystals

The amount of naphthalene crystalline deposit collected on the film on the free surface of sand layers was quantified via grayscale image intensity. The films with deposited naphthalene crystals were photographed using a DSLR camera with setting of f =7.1 and 1/5 exposition time. All images were taken under the same conditions and settings. The intensity values of each pixel in the deposition area of naphthalene crystals were measured by the open software Image J. The area occupied by the deposited crystals varied in time and with the thickness of the sand layer (cf. Fig. 3).

The original images were converted into 8-bit grayscale images. Then, the intensity values in the deposition area with deposited crystals and at the blank locations on the same film were measured. After that, the histograms of these two pixel intensities were plotted (cf. Fig. 4). The horizontal axis of the histogram represents the pixel intensity values, which range from 0 to 255, and the vertical axis of the histogram represents the corresponding number of pixels. The image in Fig. 4a corresponds to Fig. 2b. At location 1 (cf. Fig. 4a), where the crystals were observed, the pixel intensity value varies from 18 to 205 (cf. Fig. 4b), and the mean intensity value is 30.7683 ± 12.0811. No crystals were formed at location 2 (cf. Fig. 4a), and the corresponding intensity values range from 22 to 51 (cf. Fig. 4c), while the mean intensity value

is 26.6578 ± 1.5948. The values measured at location 2 were considered as the background, which means that the latter pixel intensity values should be withheld from those measured at location 1. Then, the result represents the intensity value of the crystals. This procedure was applied to all experimental images.

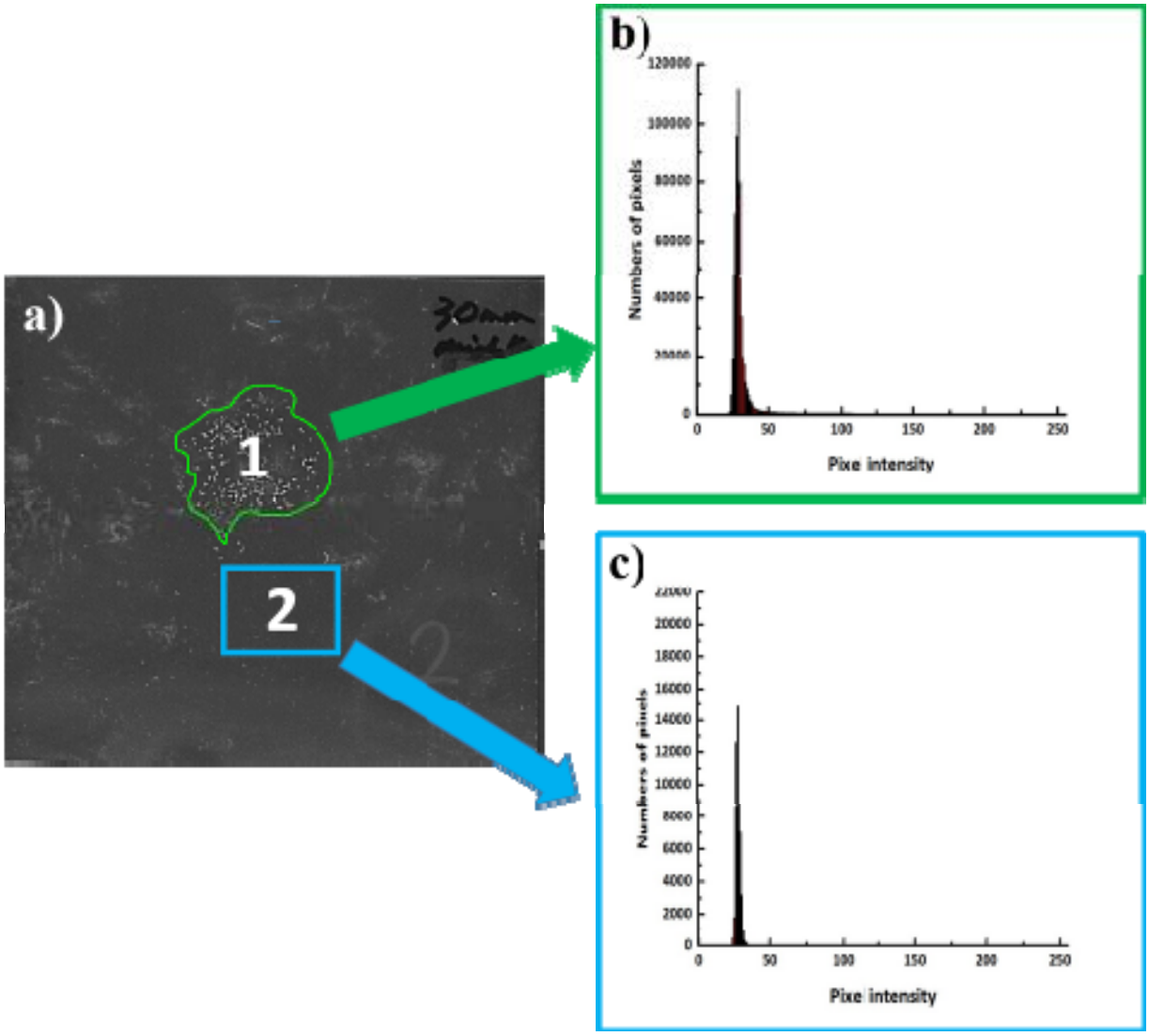

Figure 4. Measurement process of pixel values. a) The image corresponds to Fig. 2b. b) Histogram of pixel intensity versus number of pixels at position 1. c) Histogram of pixel intensity versus number of pixels at position 2.

After measuring all pixel values of the deposited crystals, as described above, the total intensity values were calculated by summing all pixel values, and then divided by the corresponding deposition area to obtain the value of the total pixel intensity per unit deposition area. Thus calculated total pixel intensity per unit area is depicted in Fig. 5 for different times and sand layer thicknesses.

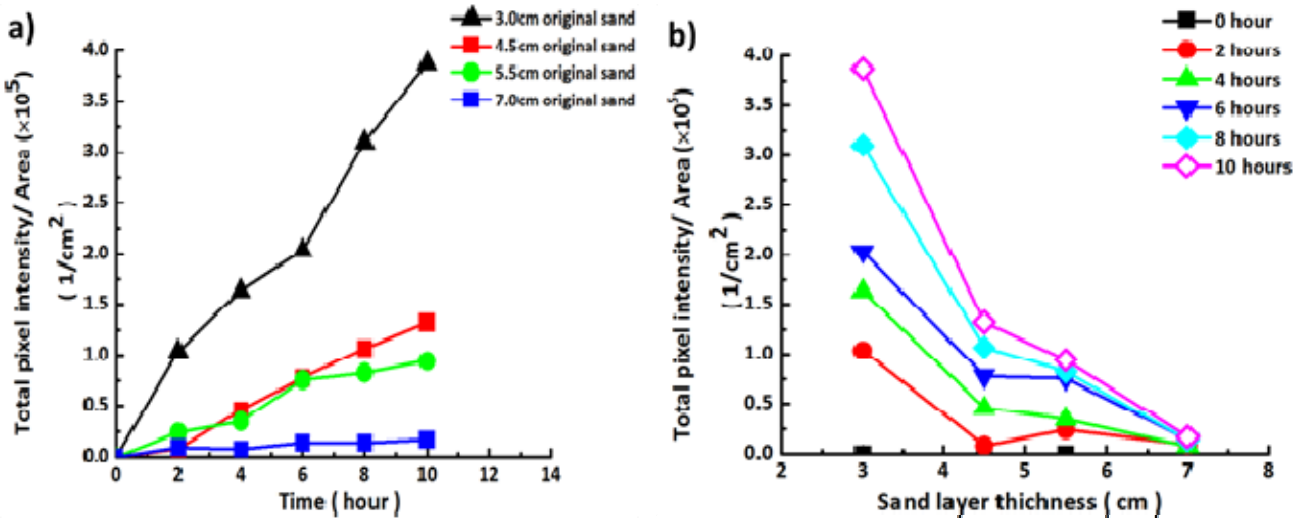

Figure 5. Total pixel intensity per unit area covered with naphthalene crystals. A 1.9 cm naphthalene ball was buried in the middle. The experiments with the original sand. (a) Total pixel intensity per unit area versus time, with time being reckoned from the delay times. (b) Total pixel intensity per unit area versus sand layer thicknesses. The experimental data is shown by symbols and spanned by lines.

It should be emphasized that measuring albedo by using photography-based methods is widely used in research and applications. However, this method can result in errors and

inaccuracies being applied to quantify vapor deposition. To compare the accuracy of the albedo method and the present image intensity method, an image taken in the experiments was used and a white paper was applied as the albedo value reference, whose value is 0.95 [28] . The values of the albedo and the corresponding total image intensity were measured at locations A and B (Fig. 6), whose areas were 1cm^2 and 0.3 cm^2, respectively. Note that the ratio of the value of an unknown object albedo to the value of a reference object albedo equals to the ratio of the brightness of the unknown object to the brightness of the reference object, and the brightness of a grayscale image is the average intensity value of all pixels in the image. At location A, the brightness value was measured as 43.507 ± 30.815, the albedo value was 0.31, and the total image intensity per unit area measured was 6208153 cm^{-2}. At location B, the brightness value was measured as 31.000 ± 24.557, the albedo value was 0.22, and the total image intensity per unit area measured was 561916 cm^{-2}. It is seen that the albedo values corresponding to locations B and A vary by only 41%, while the intensity values per unit area vary by the factor of 10 (about 1000%). These values show that the albedo method is much less sensitive to the physical changes than the image intensity method used in the present work.

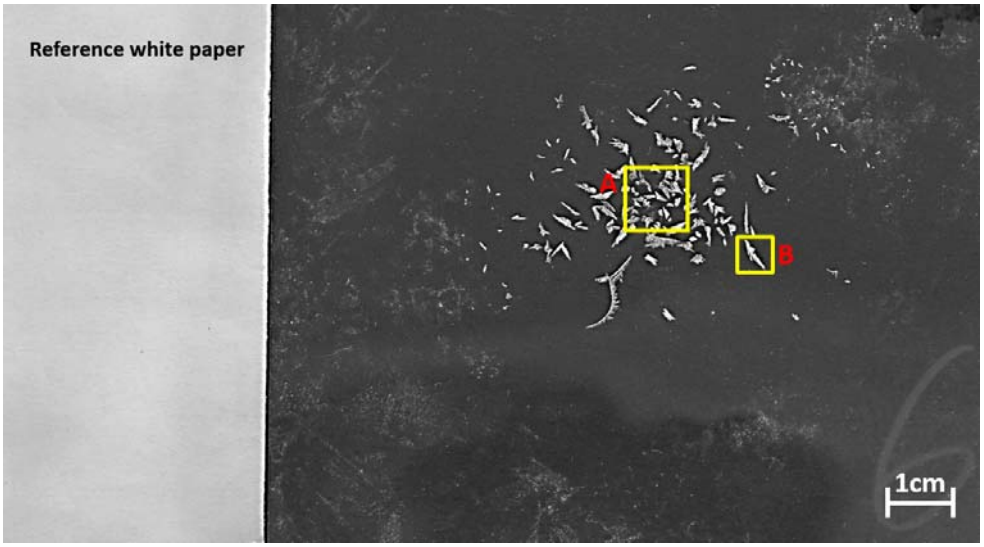

Figure 6. Comparison of the albedo method and the image intensity method. Squares indicate locations A and B used in the measurements.

2.4 Correlation of the image intensity with the deposited vapor mass

In this subsection, the correlation of the deposited vapor mass with the image intensity is established. For this goal, nine naphthalene balls of the same diameter of 1.9 cm were placed in nine separate beakers. Then, layers of h=2.0 cm thickness of sand were filled up in the beaker, and the bottom temperature of the beakers was sustained at 78 ^{o}C (below the melting temperature of naphthalene of 80.26 ^{o}C) to speed up the experiments. Nine transparent films, which were the same as in the previously described experiments, were placed on top of sand to collect the naphthalene crystals formed by the deposited vapor. The film weights were measured in 1 h, 1.5 h, 2 h and 2.5 h. The pure film weight was withheld from the measured values to find the weight of the deposited vapor as a function of time. Simultaneously, the total pixel intensity and deposition area were measured, as described in subsections 2.2 and 2.3. The mass of these

crystals was linked to the total pixel intensity, as shown in Fig. 7. The linear fit of the measured deposited mass m to the total intensity is given by the function $m = 6.61\times10^{-10}\ I_t + 0.0005$, and the standard deviations of the slope and intercept are 1.18×10^{-10} and 0.0001, respectively. The free term in this correlation is negligibly small and the correlation reduces to

$$m = 6.61\times10^{-10}\ I_t \tag{1}$$

which was used in the data processing, where m is the vapor mass in g and I_t is the total pixel intensity values.

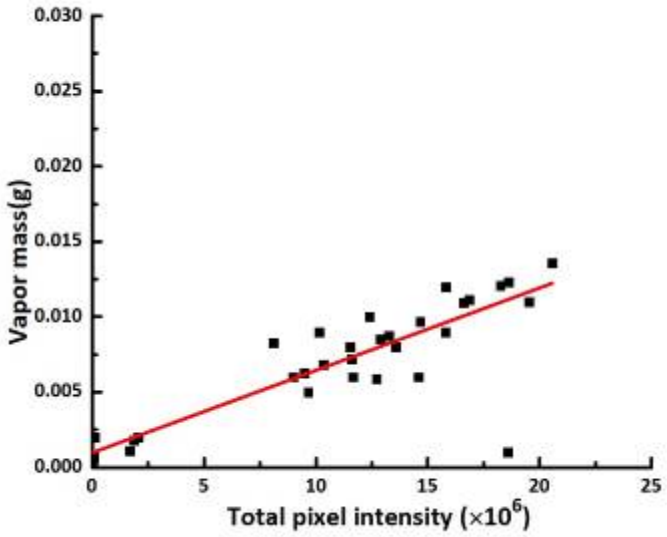

Figure 7. Deposited vapor mass versus the total intensity. The red line is the linear fit.

In addition to the experiments with naphthalene balls located at the bottom center, data was collected in the cases where the vapor source was located under the original sand off-center. These data is not discussed here for the sake of brevity.

3. Experiments with kaolinite

Kaolinite is an earthy, very soft white clay mineral. SEM images reveal that this clay has a plate-like structure (Fig. 8). Air and moisture could occupy the pores between kaolinite plates. When kaolinite has been dried, only air would be contained in the pores and the mass M of a certain volume of kaolinite would be

$$M = V_{pore}\rho_{air} + V_{clay}\rho_{clay} \tag{2}$$

where V_{pore} is the volume of pores, V_{clay} is the volume of kaolinite plates, ρ_{air} is the air density and ρ_{clay} is the kaolinite density.

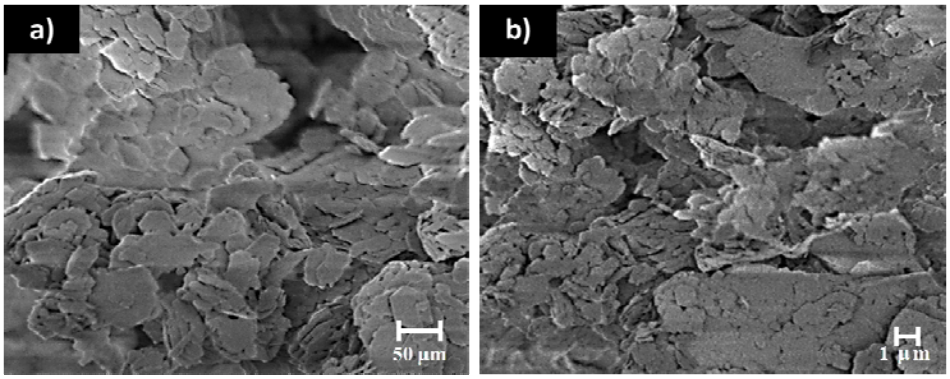

Figure 8. SEM images of plate-like structure of kaolinite.

In this section, four compacted kaolinite clay layers of thicknesses h=3.0 cm, 4.5 cm, 5.5 cm and 7.0 cm were employed. The porosity of a sample of tightly compacted kaolinite was found as 40.3%. Thus, to maintain the same porosity for four different kaolinite samples (of different thicknesses) used in the experiments, dried kaolinite mass was chosen according to Eq.

2. The clay was dried under 100 °C for 2 h. In the experiments, 397.3 g of clay was used in the h= 3.0 cm case, 596.0 g of clay was used in the h=4.5 cm case, 728.5 g of clay was used in the h=5.5 cm case and 927.1 g of clay was used in the h=7.0 cm case. The 1.9 cm naphthalene balls were buried in the middle of the tank bottom, and transparent films described in Section 2 were used to collect naphthalene depositions at the free surface of clay layers. After naphthalene crystals were first detected on the film, experiments up to 6 h -long were conducted to collect naphthalene crystals. Morphologies of the crystals at different time moments during the experiment with the kaolinite clay layer of h=3.0 cm are shown in Fig. 9.

The amount of crystals found in the experiments with kaolinite was larger than the amount in the corresponding experiments with the original sand in Section 2, and also the time t_{delay} increased. On the other hand, the naphthalene crystal size in the experiments with kaolinite was smaller compared to the experiments with the original sand in Section 2.

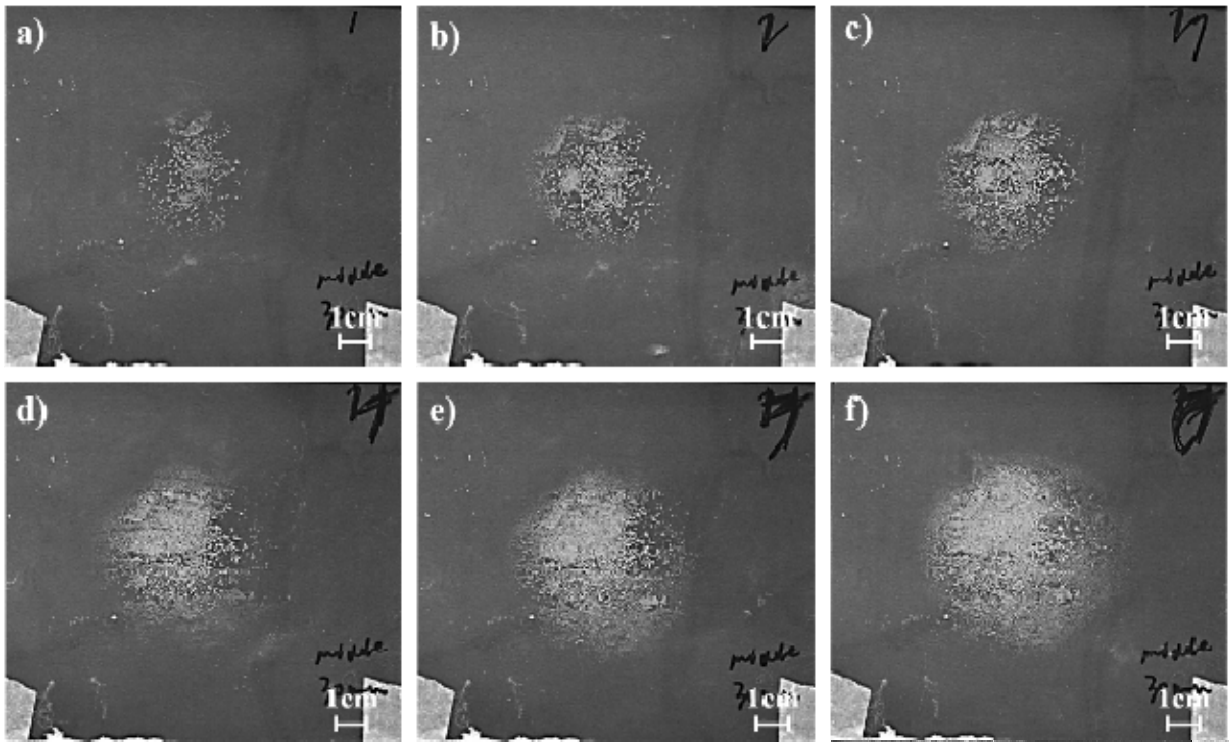

Figure 9. Morphology of naphthalene crystal deposits on transparent film at the free surface in the case of a 1.9 cm naphthalene ball buried in the middle under h=3.0 cm of kaolinite: (a) at t=1 h, (b) at t=2 h, (c) at t=3 h, (d) at t=4 h, (e) at t=5 h, (f) at t=6 h. The time is reckoned from the delay time t_{delay}= 19 h.

The area of the film with deposited crystals in the case of kaolinite porous medium obtained in 6 h reckoned after the delay time is shown in Fig. 10. The largest area values obtained at t= 6 h in the cases of h= 3.0 cm and 7.0 cm in the experiments with kaolinite are larger than those at t=8 h and 10 h in the cases of h= 3.0 cm in 7.0 cm, respectively, in the experiments with the original sand. However, the largest values obtained in the cases of h= 4.5 cm and 5.5 cm in the experiments with the original sand at t=10 h are larger than those obtained in the corresponding experiments with kaolinite.

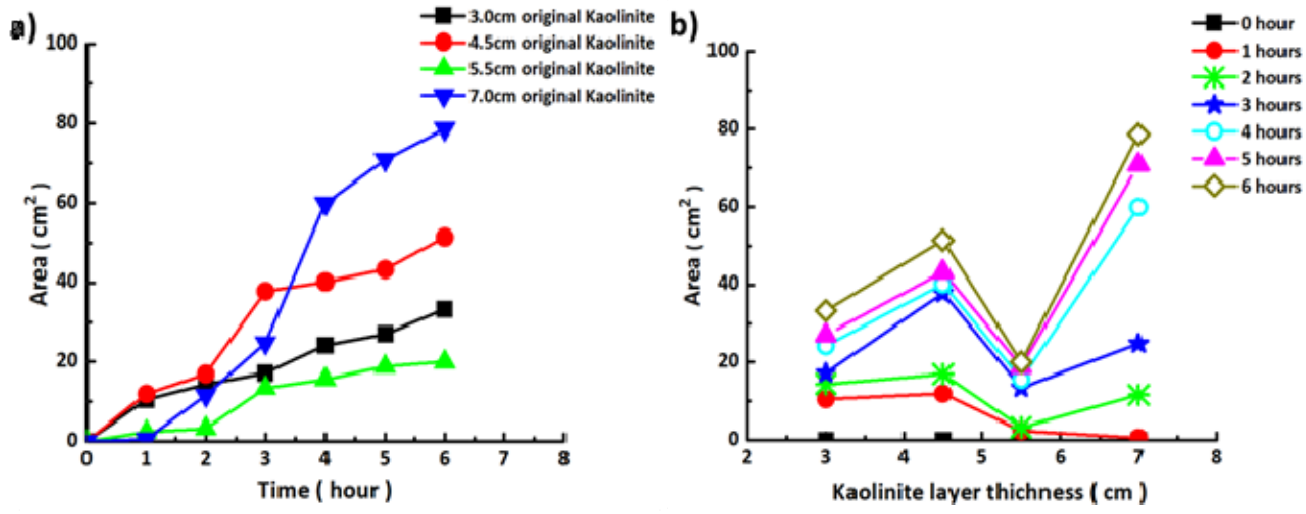

Figure 10. The measured area of the naphthalene crystal deposition. The case of the kaolinite porous medium, and a 1.9 cm naphthalene ball buried in the middle of the tank bottom. (a) The

area versus time, with time being reckoned from the delay times. (b) The area versus the kaolinite layer thickness. The experimental data is shown by symbols and spanned by lines.

The values of the total intensity per unit area with the deposited crystals in four cases in the experiments with kaolinite are shown in Fig. 11. The values obtained in each case of the layer thickness and each time moment in the experiments with kaolinite are larger than the corresponding values in the experiments with the original sand (cf. Figs. 5 and 10).

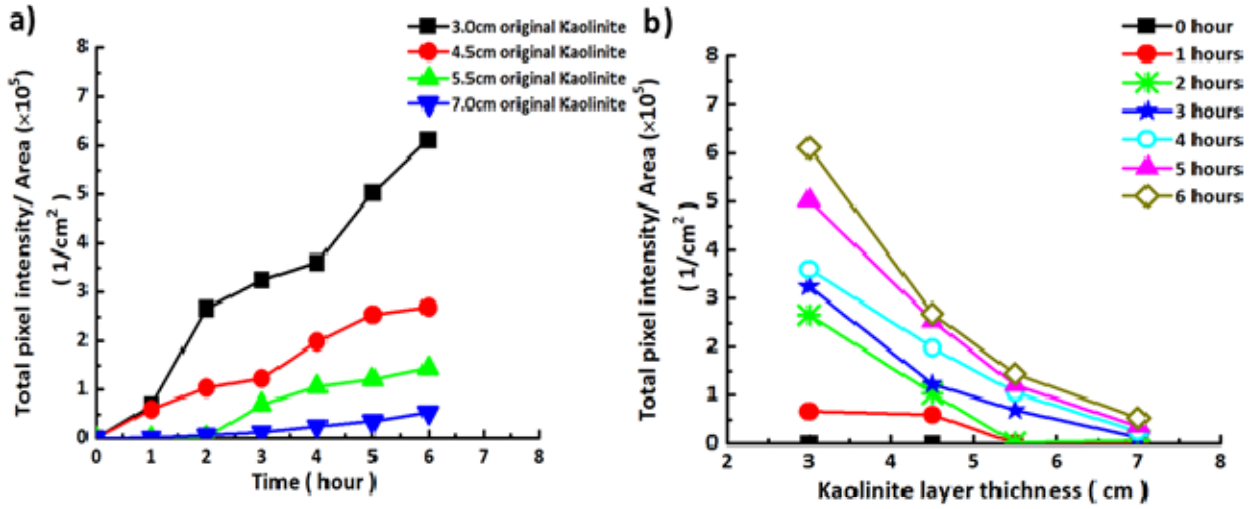

Figure 11. Total pixel intensity per unit area covered with naphthalene crystals. A 1.9 cm naphthalene ball was buried in the middle of the tank bottom. The experiments with the kaolinite layers. (a) Total pixel intensity per unit area versus time, with time being reckoned from the delay times. (b) Total pixel intensity per unit area versus the kaolinite layer thickness. The experimental data is shown by symbols and spanned by lines.

4. Theoretical

Assume that the adsorption/desorption of vapor on porous medium grains has already saturated, and the vapor transport in the pores is determined only by pure diffusion. In steady-state the diffusion equation reads

$$\frac{1}{r}\frac{\partial}{\partial r}\left(r\frac{\partial c}{\partial r}\right)+\frac{\partial^2 c}{\partial z^2}=0 \tag{3}$$

where c is vapor concentration, r is the radial coordinate, z is the vertical coordinate, and we assume an axially-symmetric process corresponding to a source buried in porous medium in the middle of the tank bottom.

Assume that a round vapor source of radius a is located at z=0 (at the bottom) with the center at r=0 (in the middle of the bottom). Over the source, the vapor concentration is known as f(r), which corresponds to sublimation, where c_w is the saturated sublimation concentration. Then, the boundary conditions for Eq. 3 read

$$c\big|_{z=0}=f(r), \quad \text{e.g.} \quad f(r)=\begin{cases} c_w \text{ at } r<a \\ 0 \text{ at } r>a \end{cases} \tag{4}$$

$$c\big|_{r\to 0}<\infty \tag{5}$$

$$c\big|_{r\to\infty,z\to\infty}<\infty \tag{6}$$

Here we imply that the porous medium extends to infinity in the radial and vertical direction, which forms a singular problem. The assumption that the medium extends to infinity is justified by the fact that the source (naphthalene ball) size is sufficiently smaller than the tank size (2a=1.9 cm versus 13 cm). The assumption that the medium extends to infinity formally holds when the layer thickness h is much larger than the source size, which is better fulfilled with h=7

cm. However, the comparison of the theory with the experimental data discussed below shows that this approximation still works when h approaches 2a.

The solution of this singular problem possesses a continuous eigenvalue spectrum ν and is found using the variable of separation method as

$$c = \int_0^\infty M_\nu e^{-\nu z} J_0(\nu r)\, d\nu \tag{7}$$

where $J_0(g)$ is the Bessel function of the first kind of zero order. The Eq. 7 already satisfies Eq. 3 and the boundary conditions 5 and 6. The coefficient M_ν is found using the boundary condition, Eq. 4

$$c\big|_{z=0} = f(r) = \int_0^\infty M_\nu J_0(\nu r)\, d\nu \tag{8}$$

This yields

$$M_\nu = \nu \int_0^\infty f(\rho)\rho J_0(\nu\rho)\, d\rho \tag{9}$$

where ρ is a dummy variable.

In particular, using the function f(r) from Eq. 4, and combining Eqs. 7 and 9, we arrive at

$$c = c_w \int_0^\infty e^{-\nu z} \nu J_0(\nu r) \int_0^a \rho J_0(\nu\rho)\, d\rho d\nu \tag{10}$$

The inner integral in Eq. 10 is easily evaluated, and Eq. 10 yields the following solution of the problem

$$c = c_w a \int_0^\infty e^{-\nu z} J_0(\nu r) J_1(\nu a)\, d\nu \tag{11}$$

At the axis of the vapor 'jet' rising by diffusion, i.e. at r=0, the integral in Eq. 11 can be evaluated analytically, which yields vapor distribution over the vertical axis z as

$$c\big|_{r=0} = c_w\left[1-\frac{z}{\sqrt{z^2+a^2}}\right] \tag{12}$$

Accordingly, the vapor flux along the axis if found as

$$-D\frac{\partial c}{\partial z}\bigg|_{r=0} = \frac{Dc_w a^2}{\left(z^2+a^2\right)^{3/2}} \tag{13}$$

where D is the diffusion coefficient.

Therefore, at a distance z from the source, at a small central area S during time t the following mass m is expected to be deposited on an inserted (or an overlying) film

$$m = \frac{Dc_w a^2 St}{\left(z^2+a^2\right)^{3/2}} \tag{14}$$

This prediction is compared below with the experimental data for the deposit masses collected on the overlying films at different distances z from the sublimating vapor source.

Note that the empirical Antoine equation,

$$\log_{10} p = A - \frac{B}{T+C} \tag{15}$$

is used to evaluated the saturated pressure of naphthalene. Here p is pressure in mm Hg, T is the temperature in ^{o}C, and A, B and C are the material-specific constants. Using the physical parameters from references [28,29], in particular, $A = 6.89116$ $B = 1551.4785$, and $C = 168.879$, one can evaluate that saturated sublimation pressure of naphthalene at $78\,^{o}C$ is p =4.2869 mm Hg,

which equals to 571.5396 Pa. Applying the ideal gas law, the saturated sublimation concentration of naphthalene in the air at $78\,^{o}C$ is evaluated as $c_w = 2.5\times10^{-5}$ g/cm^3.

The diffusion coefficient of naphthalene vapor in open air D_0 in cm^2/s at 101.325 kPa is given by the following formula [30]

$$D_0 = 0.0681\left(\frac{T}{298.16}\right)^{1.93}\left(\frac{1.013\times10^5}{p_{atm}}\right) \tag{16}$$

where T is temperature in $^{\circ}K$. The corresponding diffusion coefficient in porous medium D in cm^2/s could be calculated as [31]

$$D = D_0\varepsilon^{4/3} \tag{17}$$

where ε is the porosity of a dried porous medium. Hence, the diffusion coefficient of naphthalene vapor in the dried sand with porosity ε=0.191 (19.1%) filled with air at 352.15 $^{\circ}K$ ($78\,^{o}C$) is $0.0104\,cm^2/s$, and in kaolinite layer with porosity $\varepsilon = 0.403$ filled with air at 352.15 $^{\circ}K$ ($78\,^{o}C$) is $0.0279\,cm^2/s$.

5. Comparison of the theory with experimental data

In terms of the deposited vapor mass, determined by Eq. 1, the experimental data from Fig. 5 for the original sand layers is shown in Figs. 12 and 13 in comparison with the theoretical predictions given by Eqs. 14-17. The agreement is reasonable for all the sand layer thicknesses and time moments.

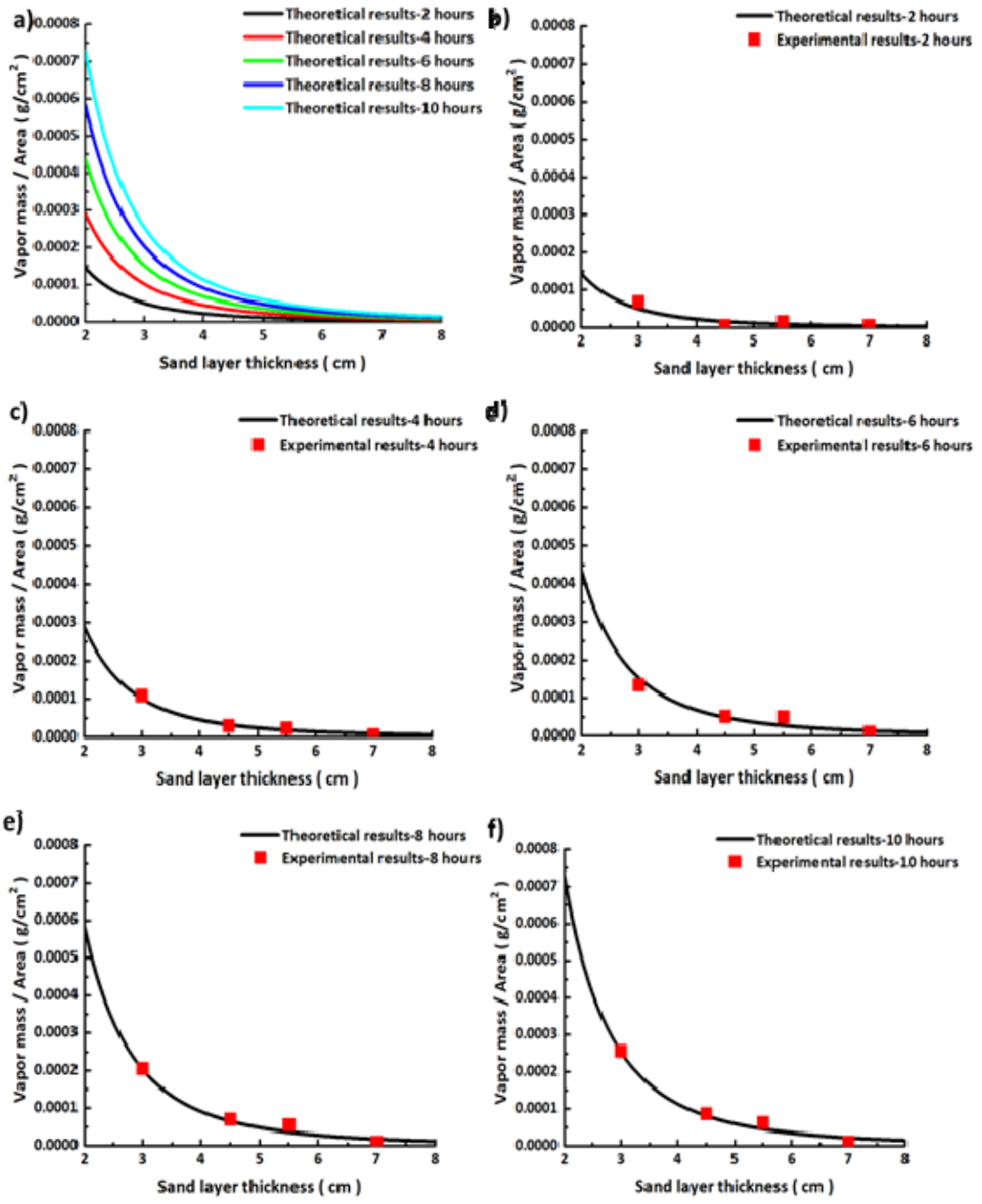

Figure 12. Naphthalene vapor mass per unit area versus the original sand layer thickness at different time moments after the adsorption/desorption process has been saturated, and vapor transport is fully determined by diffusion. (a) Theoretical results at different time moments listed in the panel. The deposited mass distribution versus the sand layer thickness. In the following

five panels the theoretical results are shown separately by lines, while the corresponding experimental data - by symbols. (b) t= 2 h. (c) t= 4 h. (d) t= 6 h. (e) t= 8 h. (f) t= 10 h.

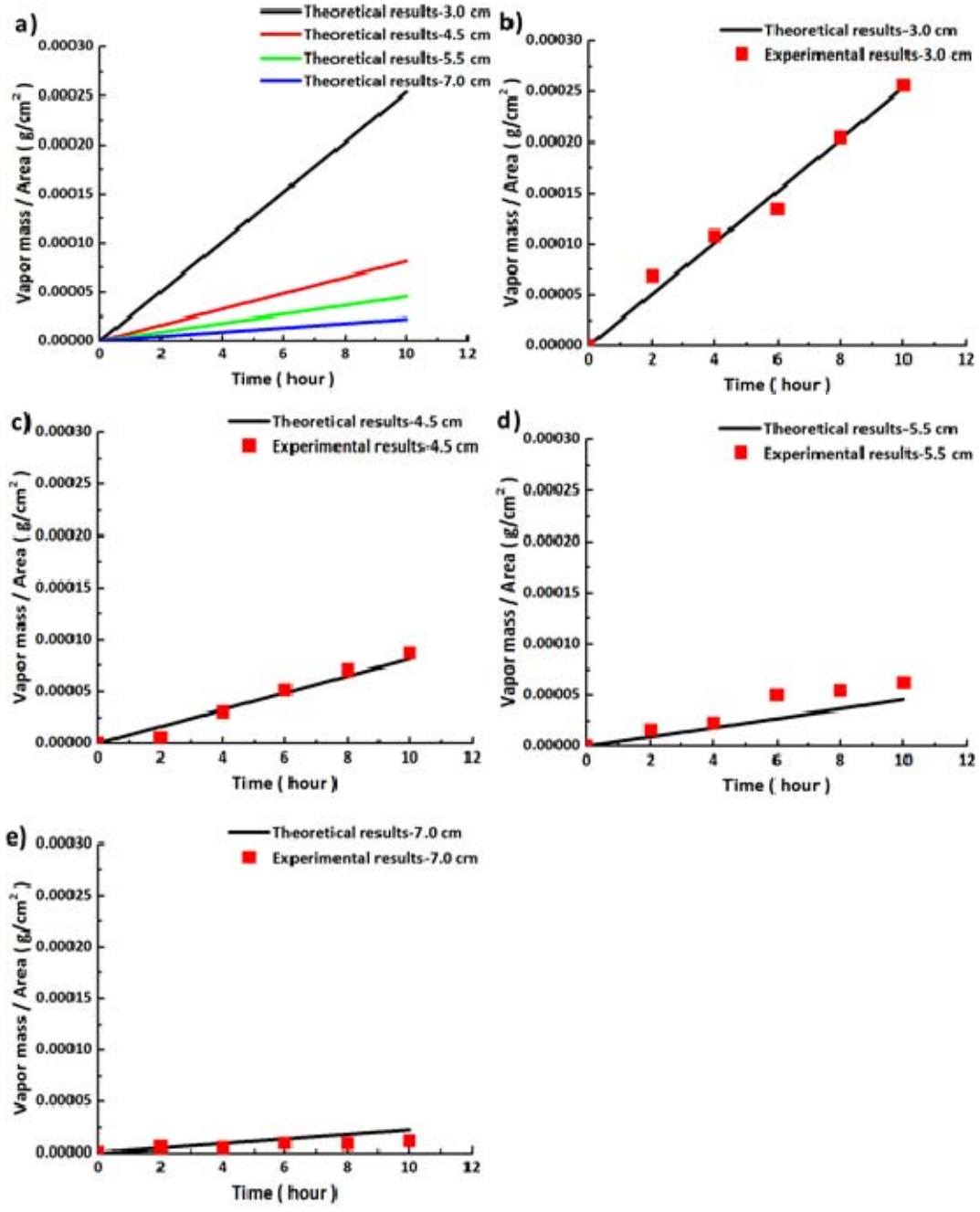

Figure 13. Naphthalene vapor mass per unit area versus time after the adsorption/desorption process has been saturated, and vapor transport is fully determined by diffusion at different

thicknesses of the original sand layers. (a) Theoretical results at different sand layer thicknesses listed in the panel. In the following four panels the theoretical results are shown separately by lines, while the corresponding experimental data - by symbols. (b) Sand layer thickness of 3.0 cm. (c) Sand layer thickness of 4.5 cm. (d) Sand layer thickness of 5.5 cm. (e) Sand layer thickness of 7.0 cm.

The experimental data from Fig. 11 for the kaolinite layers is shown in Fig. 14 and Fig. 15 in comparison with the theoretical predictions given by Eqs. 15-18. The agreement is reasonable for all the kaolinite layer thicknesses and time moments.

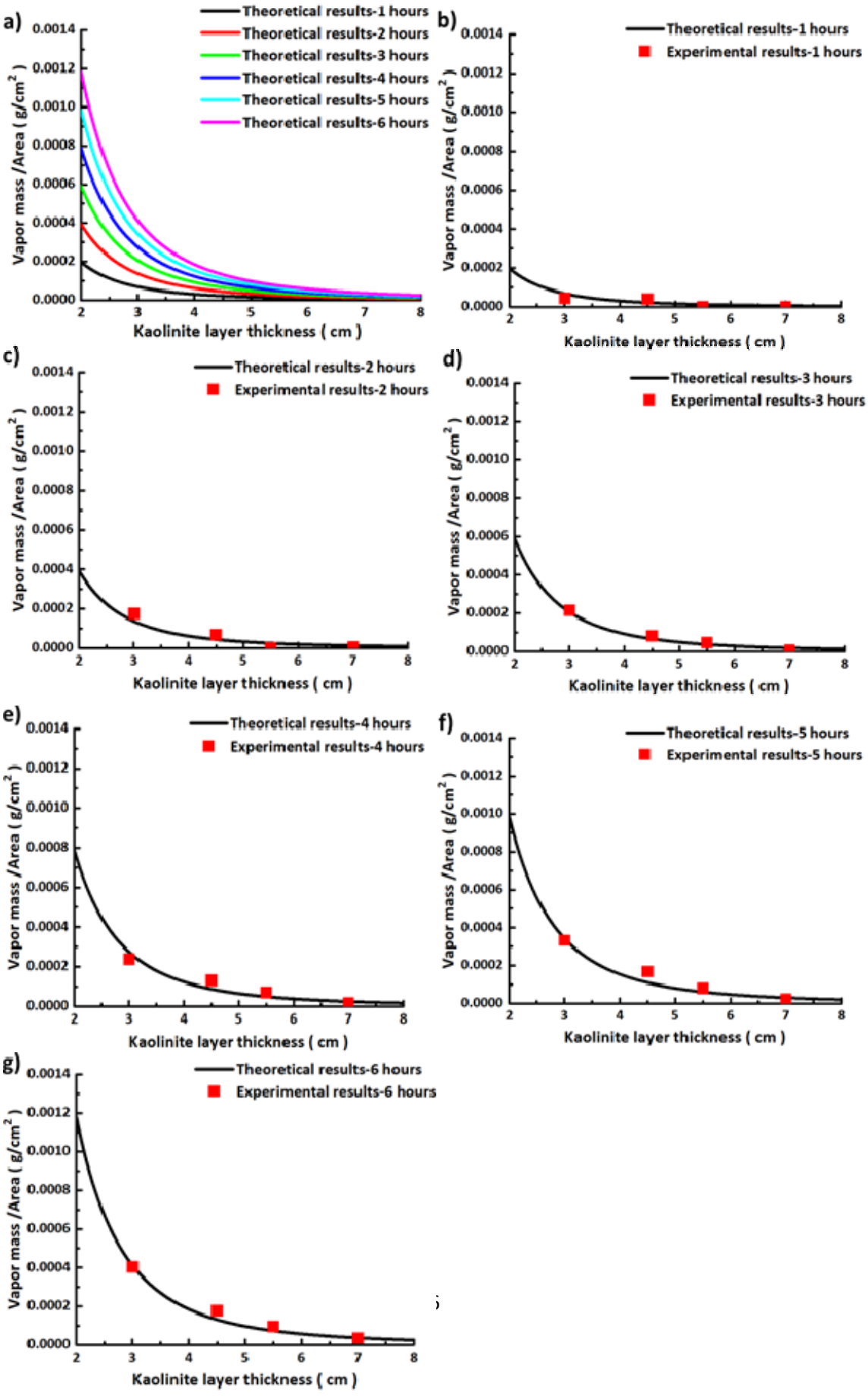
a)
Theoretical results-1 hours
Theoretical results-2 hours
Theoretical results-3 hours
Theoretical results-4 hours
Theoretical results-5 hours
Theoretical results-6 hours
Vapor mass /Area (g/cm^2)
Kaolinite layer thickness (cm)
b)
Theoretical results-1 hours
Experimental results-1 hours
c)
Theoretical results-2 hours
Experimental results-2 hours
d)
Theoretical results-3 hours
Experimental results-3 hours
e)
Theoretical results-4 hours
Experimental results-4 hours
f)
Theoretical results-5 hours
Experimental results-5 hours
g)
Theoretical results-6 hours
Experimental results-6 hours

Figure 14. Naphthalene vapor mass per unit area versus the kaolinite layer thickness at different time moments after the adsorption/desorption process has been saturated, and vapor transport is fully determined by diffusion. (a) Theoretical results at different time moments listed in the panel. The distribution of the deposited mass per unit area versus kaolinite layer thickness. In the following six panels the theoretical results are shown separately by lines, while the corresponding experimental data - by symbols. (b) t= 1 h. (c) t= 2 h. (d) t= 3 h. (e) t= 4 h. (f) t= 5 h. (g) t= 6 h.

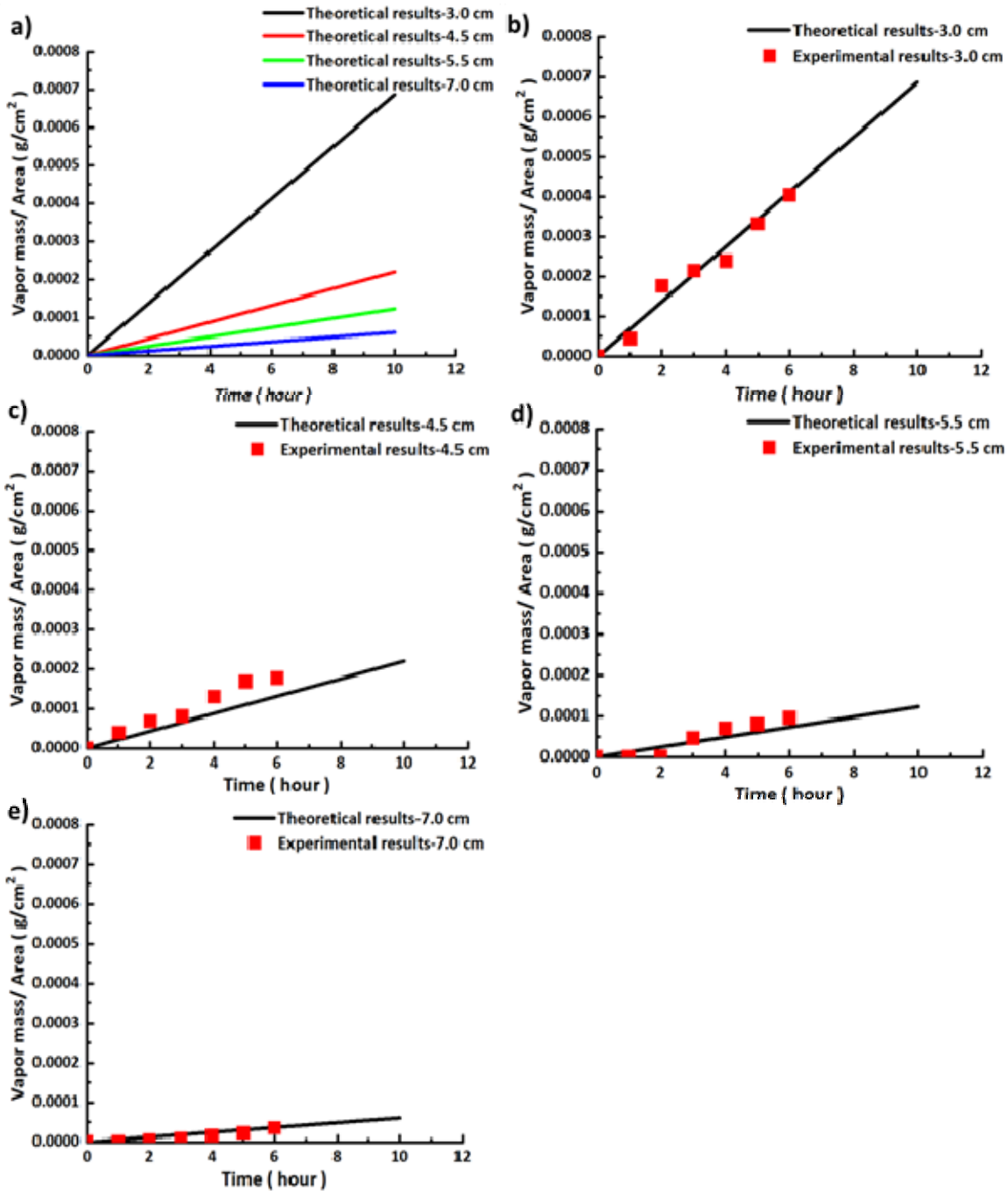

Figure 15. Naphthalene vapor mass per unit area versus time after the adsorption/desorption process has been saturated, and vapor transport is fully determined by diffusion at different thicknesses of the kaolinite layers. (a) Theoretical results at different kaolinite layer thicknesses listed in the panel. In the following four panels the theoretical results are shown separately by

lines, while the corresponding experimental data - by symbols. (b) Kaolinite layer thickness of 3.0 cm. (c) Kaolinite layer thickness of 4.5 cm. (d) Kaolinite layer thickness of 5.5 cm. (e) Kaolinite layer thickness of 7.0 cm.

It should be emphasized that Figs. 12 – 14 show the mass of naphthalene vapor released from sand layer deposited on transparent film covering the beakers per unit area. No saturation has been reached in any of these cases and currently there is no available information (either theoretical or experimental), which can allow one to evaluate the maximum possible mass collected on transparent film if the naphthalene ball would last forever.

6. Experiments with sand with coated grains

In this section vapor transport is studied using sand with coated grains, i.e. modified in comparison with the original sand studied in the Sections 2 and 5. Four different kinds of coated sand are used: sand with grains coated by naphthalene molecules, sand with grains coated by camphor molecules, sand after silanization process (hydrophobic) and sand with grains coated by a polymer. Only the latter case (polymer coating) is discussed in detail here, whereas the cases of sand with grains coated by naphthalene molecules, sand with grains coated by camphor molecules, and sand after silanization process are omitted from the discussion for the sake of brevity.

Polyacrylonitrile (PAN, (molecular weight 150 kDa) is a synthetic, semi-crystalline organic polymer. Evaporating a droplet of 5 wt% PAN dissolved in N,N-dimethylformamide

(DMF) at room temperature for a long enough time on a glass slide on a shaker, a very thin transparent film could be formed (Fig. 16). Also, being dipped into PAN solution and dried, the original sand grains stayed apart and were wrapped by a thin polymer film. This film covered the fractal-like structures on the sand grains and made them much smoother (see SEM images in Fig. 17), thus reducing the number of potential adhesion sites at the sand grain surface.

Figure 16. Transparent film formed after evaporating 0.1 g droplet of 5 wt% PAN solution in DMF.

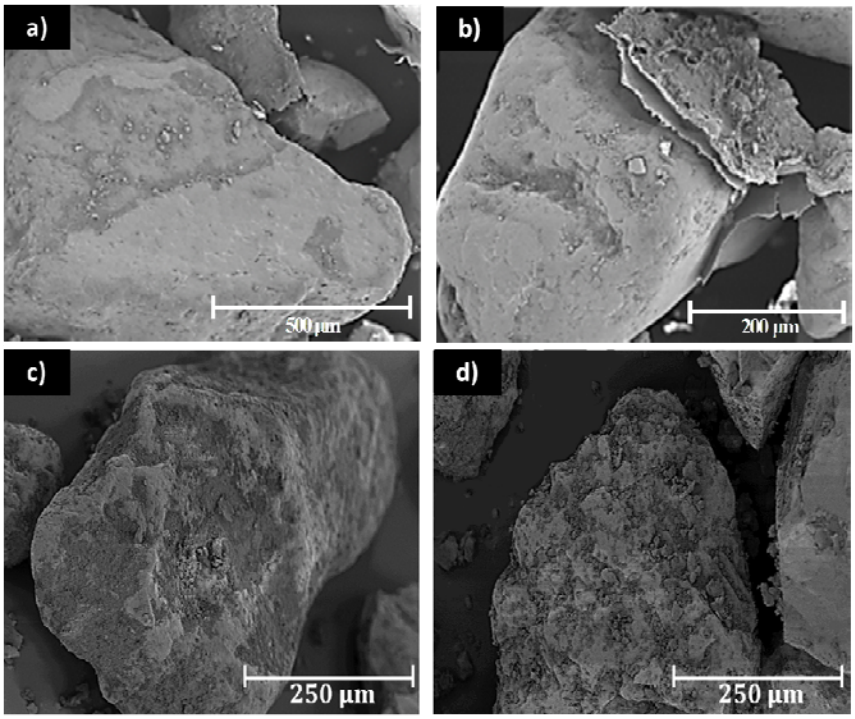

Figure 17. (a) and (b) SEM images of sand grains after they were dipped into 5 wt% PAN solution and dried. The grains are covered by a thin PAN layer and are smoother than the original sand grains in panels (c) and (d).

The polymer-coated sand was prepared using the pretreated original sand, which was dipped into 5 wt% PAN solution, fully dried, gently crushed and sieved. Both PAN and DMF were purchased from Sigma- Aldrich. The sieve opening selected was in the 0.212 mm to 1.4 mm range. Note that no DMF was left in the sand coating after drying. The average thickness of PAN coating on sand particles was approximately l =10 µm.

Four PAN-coated sand layers with thicknesses of h=3.0 cm, 4.5 cm, 5.5 cm and 7.0 cm were used in the present experiments. A 1.9 cm naphthalene ball was used as a vapor source which was buried in the middle of the tank bottom. In the case of h=3.0 naphthalene crystals could be observed in 1.5 h; in the case of h=4.5 cm, naphthalene crystals could be observed in 2.5 h; in the case of h=5.5 cm naphthalene crystals could be observed in 3 h; in the case of h=7.0 cm naphthalene crystals could be observed in 4 h. The observed morphologies of crystals in the case of the h=4 cm layer at different times are shown in Fig. 18.

In these four experiments, the film areas occupied by the deposited crystal increase as time increases. The size of the clusters formed in the experiments with the PAN-coated sand is larger than those observed in the corresponding experiments with the hydrophobic sand. However, the number of crystals deposited in experiments with the PAN-coated sand is less than in the corresponding experiments with the original sand (cf. Section 2).

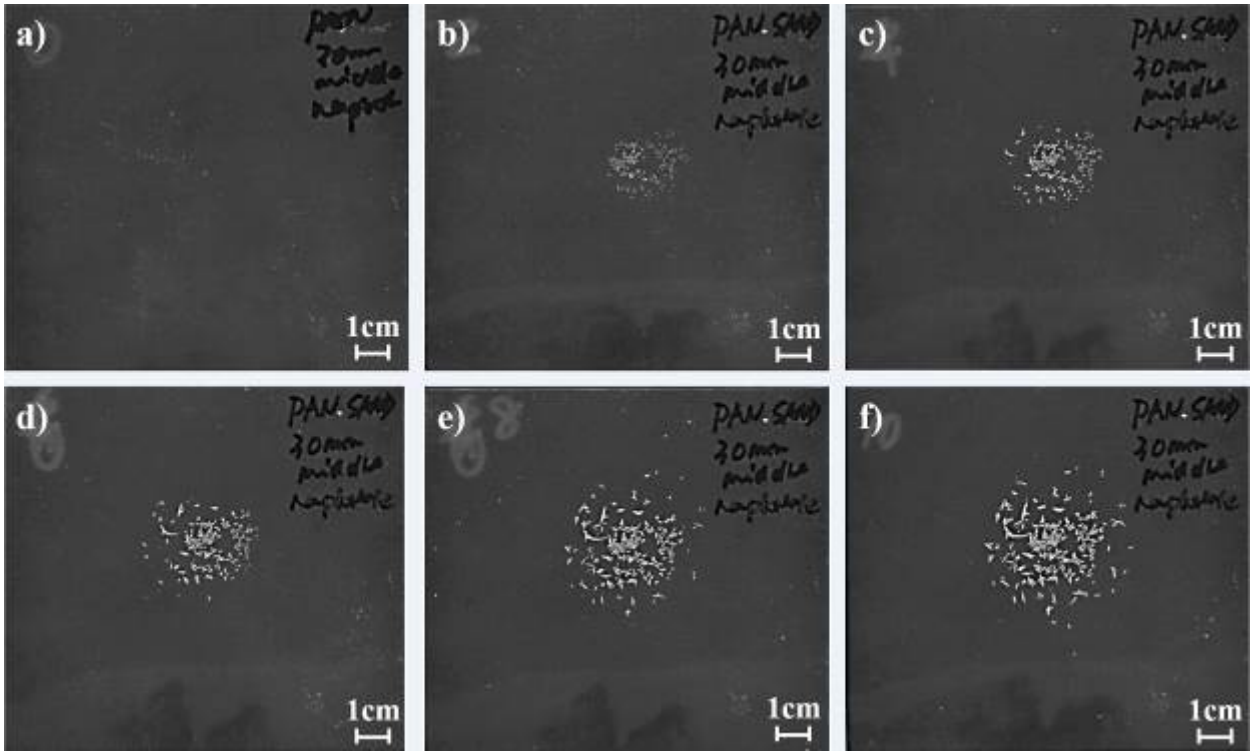

Figure 18. Morphology of naphthalene crystal deposits on transparent film at the free surface in the case of a 1.9 cm naphthalene ball buried in the middle of the tank bottom under h=3.0 cm of the PAN-coated sand: (a) at t=0, (b) at t=2 h, (c) at t=4 h, (d) at t=6 h, (e) at t=8 h, (f) at t=10 h. The time is reckoned from the delay time t_{delay}=1.5 h.

The area of the film with the deposited crystals in the case of the PAN-coated sand obtained within 10 h reckoned after the delay times is shown in Fig. 19. The area values measured in the case of the PAN-coated sand were the largest among the three types of sand explored in this work (including the original sand and the hydrophobic sand, cf. Section 2).

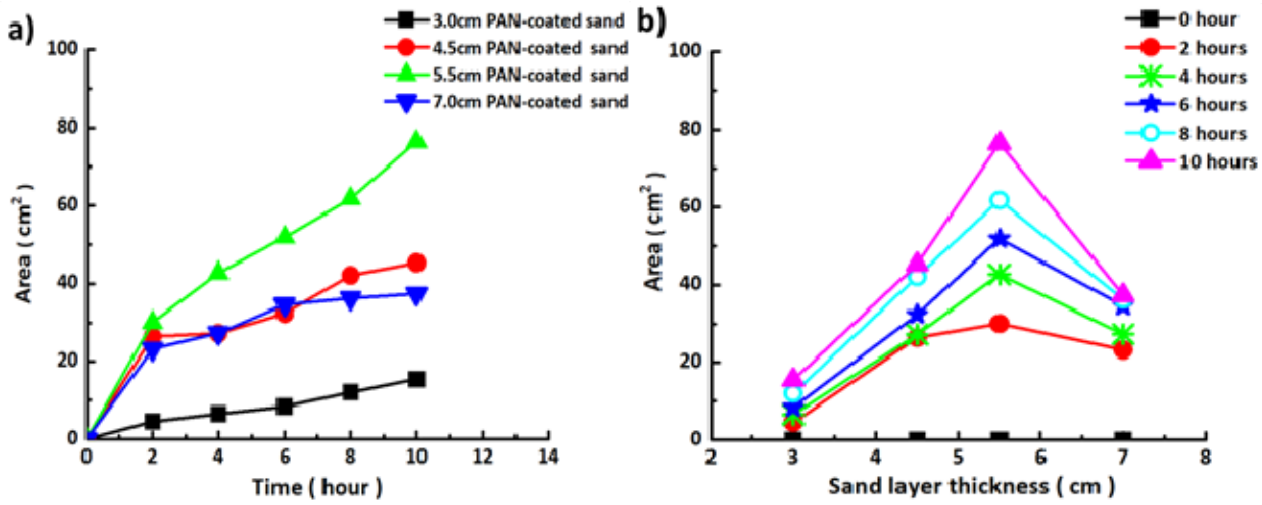

Figure 19. The measured deposit area of the naphthalene crystals deposition. The case of the PAN-coated sand, and the naphthalene ball buried in the middle of the tank bottom. (a) The area versus time, with time being reckoned from the delay times. (b) The area versus the thickness of the PAN-coated sand layers. The experimental data is shown by symbols and spanned by lines.

The values of the total pixel intensity per unit area covered with the deposited crystals in all the cases explored using the PAN-coated sand are shown in Fig. 20. The largest values of the total pixel intensity per unit area obtained in the experiments with the PAN-coated sand are smaller than the corresponding values in the experiments with the original sand (cf. Section 2) and larger than the corresponding values in the experiments with the hydrophobic sand.

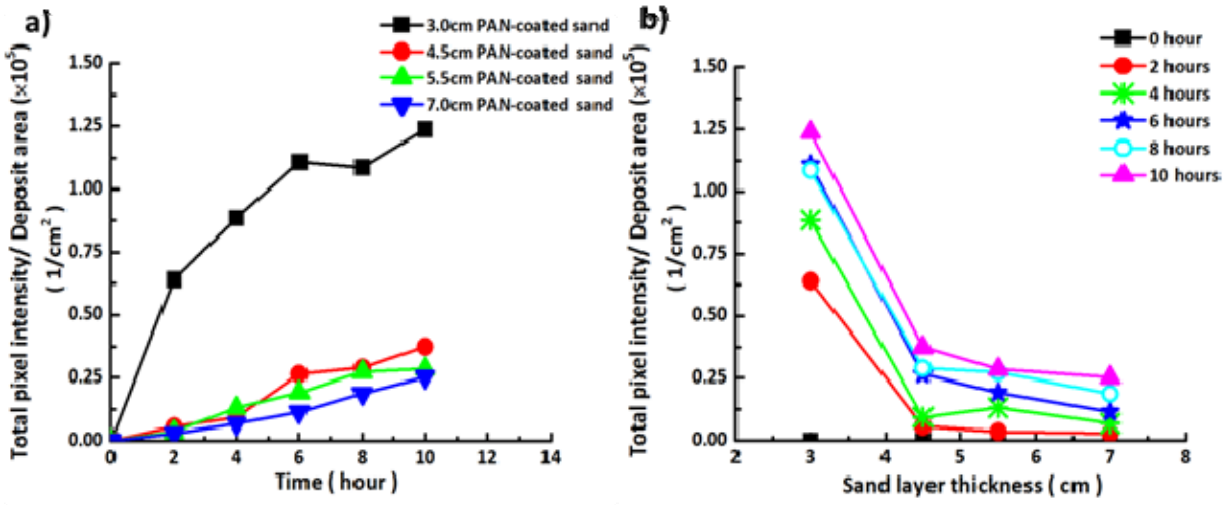

Figure 20. Total pixel intensity per unit area covered with naphthalene crystals. The naphthalene ball was buried in the middle of the tank bottom. The experiments with the PAN-coated sand. (a) Total pixel intensity per unit area versus time, with time being reckoned from the delay times. (b) Total pixel intensity per unit area versus sand layer thickness. The experimental data is shown by symbols and spanned by lines.

The values of the total pixel intensity per unit area in all the cases studied using the original sand (Section 2), the hydrophobic sand and the PAN-coated sand are summarized in Fig. 21. It is clear that the delay time could be decreased by modifying sand, especially after coating it with 5

wt% PAN solution, in comparison to the delay time corresponding to the original sand. The delay time results from the adsorption of naphthalene vapor on sand grains, which precludes vapor release to the free surface. Accordingly, the prolonged adsorption of vapor on sand grains delays its detection at the free surface.

The very fact that the presence of PAN coating results in a faster vapor release to the free surface means that such coating significantly diminishes retainment of the vapor inside sand layer. Therefore, if there would be any adsorption of naphthalene vapor on PAN, it would be much less than on sand. Also, vapor diffusion into PAN layer is hardly a factor. Indeed, the characteristic time of such diffusion $\tau_D \sim l^2 / D_{PAN}$, with D_{PAN} being the diffusion coefficient in solid PAN, is of the order 10 h, since $D_{PAN} \sim 10^{-10} cm^2 / s$ [33]. This time is longer than the delay in the significant vapor release to the free surface. Therefore, significant accumulation of naphthalene vapor inside PAN layer is excluded. On the other hand, coating sand grains (e.g. with PAN layer) significantly decreases the surface area of individual sand grains available for the adsorption, since the grain surface is dramatically smoothened, as seen in Fig. 17 in the revised version. Therefore, vapor almost immediately reaches by diffusion the free surface (Fig. 21) where it can be detected.

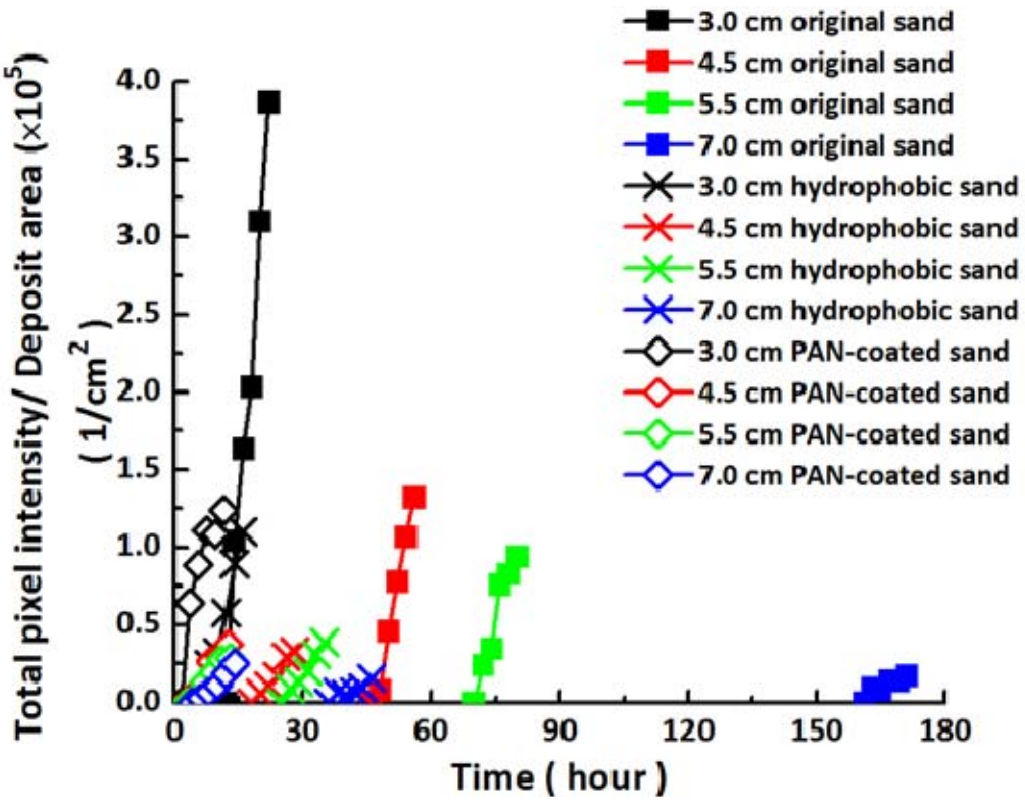

Figure 21. Total pixel intensity per unit area covered with naphthalene crystals. A 1.9 cm naphthalene ball was buried in the middle of the tank bottom. The experiments with the original sand, the hydrophobic sand and the PAN-coated sand. The experimental data is shown by symbols and spanned by lines.

7. Conclusion

A method of measurement of vapor mass deposited by vapor sublimated from a buried source and diffused through a porous media, such as sand or a kaolinite layer is proposed. The theory predicting mass deposition on a detector located at the free surface is also proposed and compared with the experimental data with the original sand and kaolinite layers. The agreement of the theoretical predictions with the experimental data is rather good. In addition, the

experiments with two kinds of modified sands were conducted: with the hydrophobic sand with a thin trimethylsilanol layer at the grain surfaces, and with the polymer-coated sand with a thin PAN layer at the grain surfaces. It is shown that the deposited layers make the grains smoother and significantly diminish the surface area available for molecular adsorption. The latter significantly accelerates the release of the vapor sublimating from the buried source to the free surface where it can be detected.

Corresponding Author

* E-mail: ayarin@uic.edu

* E-mail: meeyal@me.technion.ac.il

References

[1] H. Zhang, W. Gu, M. J. Li, Z. Y. Li, Z. J. Hu, W. Q. Tao. Experimental Study on the Kinetics of Water Vapor Sorption on the Inner Surface of Silica Nano-porous Materials. International Journal of Heat and Mass Transfer. 78 (2014): 947-959.

[2] R. L. Cleland. Adsorption from Nonelectrolyte Solutions on Porous 96% Silica (Vycor) Glass. The Journal of Physical Chemistry. 68 (1964): 1432-1438.

[3] K. Ignatowicz. A Mass Transfer Model for the Adsorption of Pesticide on Coconut Shell Based Activated Carbon. International Journal of Heat and Mass Transfer. 54 (2011): 4931-4938.

[4] A. Sánchez-Sánchez, F. Suárez-García, A. Martínez-Alonso, J. M. Tascón. Influence of Porous Texture and Surface Chemistry on the CO_2 Adsorption Capacity of Porous Carbons: Acidic and Basic Site Interactions. ACS Applied Materials & Interfaces. 6 (2014): 21237-21247.

[5] A. Kolbasov, S. Sinha-Ray, A. L. Yarin, B. Pordeyhimi. Heavy Metal Adsorption on Solution-blown Biopolymer Nanofiber Membranes. J. Membrane Sci. 530 (2017): 250-263.

[6] Q. Y. Zhu, M. H. Xie, J. Yang, Y. Li. A Fractal Model for the Coupled Heat and Mass Transfer in Porous Fibrous Media. International Journal of Heat and Mass Transfer. 54 (2011): 1400-1409.

[7] I. Langmuir. The Adsorption of Gases on Plane Surfaces of Glass, Mica and Platinum, J. Am. Chem. Soc. 40 (1918): 1361–1403.

[8] S. Brunauer, P. H. Emmett, E. Teller. Absorption of Gases in Multimolecular Layers. J. Am. Chem. Soc. 60 (1938): 309-319.

[9] X. Zhu, Y. Shi, N. Cai. High-pressure Carbon Dioxide Adsorption Kinetics of Potassium-modified Hydrotalcite at Elevated Temperature. Fuel. 207 (2017): 579-590.

[10] X. Yang, Y. Li, C. T. Lira. Kinetics Modeling of Adsorption and Desorption of Benzaldehyde and Benzyl Alcohol on Polymeric Resin in Supercritical CO_2. Journal of CO_2 Utilization. 21 (2017): 253-260.

[11] E. Osagie, C. N. Owabor. Adsorption of Benzene in Batch System in Natural Clay and Sandy Soil. Advances in Chemical Engineering and Science. 5 (2015): 352-361.

[12] J. W. Grate, B. M. Wise, M. H. Abraham. Method for Unknown Vapor Characterization and Classification Using a Multivariate Sorption Detector. Initial Derivation and Modeling Based on Polymer-coated Acoustic Wave Sensor Arrays and Linear Solvation Energy Relationships. Analytical Chemistry. 71 (1999): 4544-4553.

[13] J. W. Swinnerton, V. J. Linnenbom, C. H. Cheek. Determination of Dissolved Gases in Aqueous Solutions by Gas Chromatography. Analytical Chemistry. 34 (1962): 483-485.

[14] J. Theiler, B. Wohlberg. Detection of Unknown Gas-phase Chemical Plumes in Hyperspectral Imagery. Proc. SPIE. 8743 (2013): 874315.

[15] S. J. Toal, W. C. Trogler. Polymer Sensors for Nitroaromatic Explosives Detection. Journal of Materials Chemistry. 16 (2006): 2871-2883.

[16] T. Thundat, G. Y. Chen, R. J. Warmack, D. P. Allison, E. A. Wachter. Vapor Detection Using Resonating Microcantilevers. Analytical Chemistry. 67 (1995): 519-521.

[17] E. S. Snow, F. K. Perkins, J. A. Robinson. Chemical Vapor Detection Using Single-walled Carbon Nanotubes. Chemical Society Reviews. 35 (2006): 790-798.

[18] J. Li, Y. Lu, Q. Ye, M. Cinke, J. Han, M. Meyyappan. Carbon Nanotube Sensors for Gas and Organic Vapor Detection. Nano Letters. 3 (2003): 929-933.

[19] J. Zhu, L. Jacobson, D. Schmidt, R. Nicolai. Daily Variations in Odor and Gas Emissions from Animal Facilities. Applied Engineering in Agriculture. 16 (2000): 153-158.

[20] D. S. Liscinsky, Z. Yu, B. True, J. Peck, A. C. Jennings, H. W. Wong, R. C. Miake-Lye. Measurement of Naphthalene Uptake by Combustion Soot Particles. Environmental Science & Technology. 47 (2013); 4875-4881.

[21] M. M. Rhead, R. D. Pemberton. Sources of Naphthalene in Diesel Exhaust Emissions. Energy & Fuels. 10 (1996): 837-843.

[22] X. Cheng, A. T. Kan, M. B. Tomson. Naphthalene Adsorption and Desorption from Aqueous C_{60} Fullerene. Journal of Chemical & Engineering Data. 49 (2004): 675-683.

[23] W. Zhang, R. Vilensky, E. Zussman, A.L. Yarin. Adsorption and Mass Transfer in Granular Porous Membranes/Media due to Inserted Volatile Materials. International Journal of Heat and Mass Transfer. 116 (2018): 248-258.

[24] R. E. Payne. Albedo of the Sea Surface. Journal of the Atmospheric Sciences. 29 (1972): 959-970.

[25] M. D. King, M. G. Strange, P. Leone, L. R. Blaine. Multiwavelength Scanning Radiometer for Airborne Measurements of Scattered Radiation within Clouds. Journal of Atmospheric and Oceanic Technology. 3 (1986): 513-522.

[26] J. G. Corripio. Snow Surface Albedo Estimation Using Terrestrial Photography. International Journal of Remote Sensing. 25 (2004): 5705-5729.

[27] A. Troccoli, P. K. Allen. Recovering Illumination and Texture Using Ratio Images. 3D Data Processing, Visualization, and Transmission, Third International Symposium on. IEEE, 2006: 655-662.

[28] R. Carpenter, B. Reddi. Neurophysiology: A Conceptual Approach. CRC Press, 2012.

[29] R. C. Weast, J.A. Melvin, W. H. Beyer. CRC Handbook of Chemistry and Physics. CRC Press, Boca Raton, 1988. Vol. 69.

[30] C. L. Yaws. The Yaws Handbook of Vapor Pressure: Antoine Coefficients. Gulf Professional Publishing, Houston, 2015.

[31] R. J. Goldstein, H. H. Cho. A Review of Mass Transfer Measurements Using Naphthalene Sublimation. Experimental Thermal and Fluid Science. 10 (1995): 416-434.

[32] E. A. Davidson, S. E. Trumbore. Gas Diffusivity and Production of CO_2 in Deep Soils of the Eastern Amazon. Tellus B: Chemical and Physical Meteorology. 47 (1995): 550–565.

[33] G.T. Fieldson, T.A. Barbari. The Use of FTi.r.-a.t.r Spectroscopy to Characterize

Penetrant Diffusion in Polymers. Polymer. 34 (1993): 1146-1153.